Journal of The Electrochemical Society, **158** (3) A215-A222 (2011)
0013-4651/2010/158(3)/A215/8/$28.00 © The Electrochemical Society

Modeling All-Solid-State Li-Ion Batteries

D. Danilov,[a] R. A. H. Niessen,[b] and P. H. L. Notten[a,*,z]

[a]*Eindhoven University of Technology, Den Dolech 2, 5600 MB Eindhoven, The Netherlands*
[b]*Philips Research Laboratories, High Tech Campus 4, 5656 AE Eindhoven, The Netherlands*

A mathematical model for all-solid-state Li-ion batteries is presented. The model includes the charge transfer kinetics at the electrode/electrolyte interface, diffusion of lithium in the intercalation electrode, and diffusion and migration of ions in the electrolyte. The model has been applied to the experimental data taken from a 10 μAh planar thin-film all-solid-state Li-ion battery, produced by radio frequency magnetron sputtering. This battery consists of a 320 nm thick polycrystalline $LiCoO_2$ cathode and a metallic Li anode separated by 1.5 μm Li_3PO_4 solid-state electrolyte. Such thin-film batteries are nowadays often employed as power sources for various types of autonomous devices, including wireless sensor nodes and medical implants. Mathematical modeling is an important tool to describe the performance of these batteries in these applications. The model predictions agree well with the galvanostatically measured voltage profiles. The simulations show that the transport limitations in the solid-state electrolyte are considerable and amounts to at least half of the total overpotential. This contribution becomes even larger when the current density reaches 0.5 mA cm^{-2} or higher. It is concluded from the simulations that significant concentration gradients develop in both the positive electrode and the solid-state electrolyte during a high current (dis)charge.
 [DOI: 10.1149/1.3521414]

Manuscript submitted August 16, 2010; revised manuscript received November 5, 2010. Published December 28, 2010.

All-solid-state batteries are a quickly growing multimillion-dollar business, which nowadays have a large beneficial impact on many applications, such as autonomous devices for ambient intelligence and medical implants. To describe the performance of these batteries under various conditions, mathematical modeling of the Li-ion system was initiated in the mid-1980s. Simulating discharge voltage curves of Li-ion batteries already dates back to the early 1980s.[1] Interesting reviews dealing with the mathematical modeling of Li-ion batteries can be found in the literature.[2-5] These models are mainly based on the porous electrode theory developed by Newman.[6]

Alternatively, equivalent electronic network models have been presented for various types of rechargeable batteries.[7-11] All these models are based on the macroscopic descriptions of the fundamental electrochemical and physical processes occurring inside these systems, enabling the quantification of the relevant processes. The electronic network models were elegantly used to visualize these processes. Good agreement between the simulations and experimental results was reported.[7-11] In addition, the degradation (aging) process of Li-ion batteries has also been addressed.[12,13] However, all these reports did not address thin-film all-solid-state Li-ion batteries.

Solid-state Li-ion batteries represent the state-of-the-art in modern battery technology. Further improvement in the solid-state battery technology requires an in-depth understanding of the electrochemical processes involved, and the ability to simulate these processes is therefore a necessity. The ionically conductive solid-state electrolytes play an important role in the solid-state battery design (see Bates et al.[14,15]). Construction of a consistent mathematical model describing the conductivity in the solid-state electrolyte therefore forms an essential part of these models. A majority of all-solid-state Li-ion batteries have a flat thin-film design. An example of the cross section of an as-deposited solid-state Li-ion battery is given in Fig. 1a.

The aim of the current paper is to develop a mathematical model for all-solid-state Li-ion batteries, which includes all important physical and electrochemical characteristics and is capable of describing the basic functionality of these devices under a wide variety of operating conditions.

Theoretical Considerations

Electrochemical description.— A conventional solid-state Li-ion battery consists of the following elements (Fig. 1b). The negative electrode comprises metallic lithium. The positive electrode is based on the conventional $LiCoO_2$ chemistry. The electrodes are separated by a solid-state electrolyte consisting of (either or not N-doped) an amorphous Li_3PO_4. Current collectors are placed on the outer sides of each electrode. Their influence on the electrochemical processes is considered to be negligible. In line with the battery morphology (Fig. 1a), a one-dimensional approach is adopted in the present work.

The basic electrochemical charge transfer reactions at the positive and negative electrodes can be represented by

$$LiCoO_2 \underset{k_{-1}}{\overset{k_1}{\rightleftarrows}} Li_{1-x}CoO_2 + xLi^+ + xe^- \quad (0 \leqslant x \leqslant 0.5) \qquad [1]$$

$$Li \underset{k_{-2}}{\overset{k_2}{\rightleftarrows}} Li^+ + e^- \qquad [2]$$

respectively. The positive electrode generally consists of trivalent cobaltoxide species, in which the lithium ions are intercalated ($LiCo^{III}O_2$) to provide electroneutrality. During charging, the trivalent cobalt is oxidized into four-valent cobalt ($Co^{IV}O_2$) and the excess of positive charge is liberated from the electrode in the form of Li^+ ions. The Li^+ ions cross the electrolyte and are reduced into metallic Li at the negative electrode. The reverse reactions take place during discharging.

Charge transfer kinetics.— Considering the discrete valence states for the Co^{II}/Co^{IV} redox couple, the number of electrons (n) transferred is unity. Denoting k_1 and k_{-1} as the forward and backward reaction rate constants, respectively, the partial anodic (I_a) and cathodic currents (I_c) at the electrode surface can be represented by

$$I_a = FAk_1 a^s_{LiCoO_2} \qquad [3a]$$

$$I_c = FAk_{-1} a^s_{CoO_2} a^s_{Li^+} \qquad [3b]$$

where F is the Faraday constant (96,485 C mol^{-1}), A is the electrode surface area (m^2), and a^s_i is the (surface) activity of species i (mol m^{-3}). The reaction rate constants are a function of the electrode potential,[16] according to

$$k_1 = k^0_1 e^{\alpha_{LiCoO_2}(F/(RT))E_{LiCoO_2}} \qquad [4a]$$

$$k_{-1} = k^0_{-1} e^{-(1-\alpha_{LiCoO_2})(F/(RT))E_{LiCoO_2}} \qquad [4b]$$

where R is the gas constant (8.314 J mol^{-1} K^{-1}), T is the absolute temperature (K), and α_{LiCoO_2} is the charge transfer coefficient for reaction Eq. 1. Introducing these equations into Eqs. 3a and 3b yields

* Electrochemical Society Active Member.
z E-mail: p.h.l.notten@tue.nl

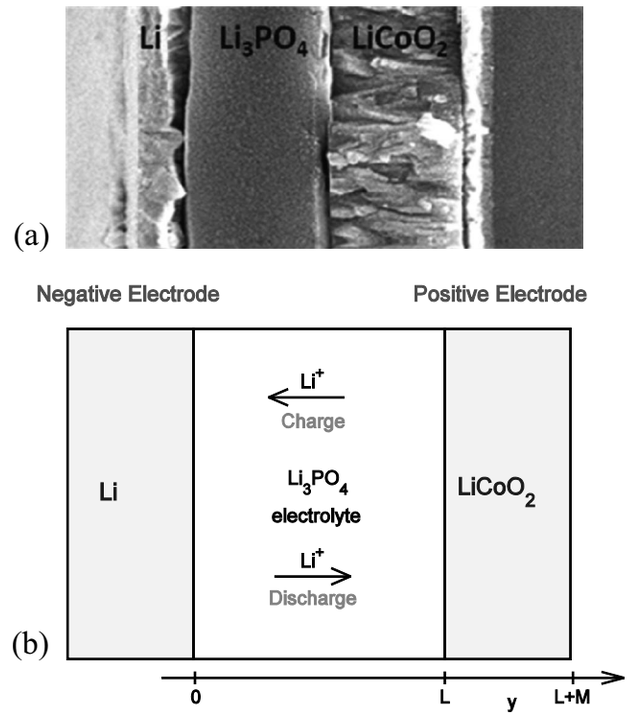

Figure 1. An example of an SEM image of an as-produced solid-state Li-ion battery (a) and general representation of a planar all-solid-state Li-ion battery (b).

$$I_a = FAa^s_{LiCoO_2}k^0_1 e^{\alpha_{LiCoO_2}(F/(RT))E_{LiCoO_2}} \quad [5a]$$

$$I_c = FAa^s_{CoO_2}a^s_{Li^+}k^0_{-1}e^{-(1-\alpha_{LiCoO_2})(F/(RT))E_{LiCoO_2}} \quad [5b]$$

The exchange current $I^0_{LiCoO_2}$ is defined at the equilibrium potential where $I_a = I_c$. Under equilibrium conditions, no concentration profiles are present and hence all the surface activities are equal to the average bulk activities ($\bar{a}_i$), i.e., $a^s_i = \bar{a}_i$. From Eqs. 5a and 5b, it follows that under this condition, $I^0_{LiCoO_2}$ can be represented by

$$\begin{aligned} I^0_{LiCoO_2} &= FA\bar{a}_{LiCoO_2}k^0_1 e^{\alpha_{LiCoO_2}(F/(RT))E^{eq}_{LiCoO_2}} \\ &= FA\bar{a}_{CoO_2}\bar{a}_{Li^+}k^0_{-1}e^{-(1-\alpha_{LiCoO_2})(F/(RT))E^{eq}_{LiCoO_2}} \end{aligned} \quad [6]$$

An expression for the equilibrium potential ($E^{eq}_{LiCoO_2}$) can then be obtained from Eq. 6

$$E^{eq}_{LiCoO_2} = \frac{RT}{F}\ln\frac{k^0_{-1}\bar{a}_{CoO_2}\bar{a}_{Li^+}}{k^0_1\bar{a}_{LiCoO_2}} = \frac{RT}{F}\ln\frac{k^0_{-1}}{k^0_1} + \frac{RT}{F}\ln\frac{\bar{a}_{CoO_2}\bar{a}_{Li^+}}{\bar{a}_{LiCoO_2}} \quad [7]$$

which is recognized as the Nernst equation. The first term on the right-hand side represents the standard redox potential and the second term takes into account the concentration dependence of the electrode potential. Eliminating $E^{eq}_{LiCoO_2}$ in Eq. 6, using Eq. 7, leads to a general expression for $E^0_{LiCoO_2}$

$$\begin{aligned} I^0_{LiCoO_2} &= FA(k^0_{-1})^{\alpha_{LiCoO_2}}(k^0_1)^{(1-\alpha_{LiCoO_2})} \\ &\quad \times(\bar{a}_{CoO_2}\bar{a}_{Li^+})^{\alpha_{LiCoO_2}}(\bar{a}_{LiCoO_2})^{(1-\alpha_{LiCoO_2})} \\ &= FAk^s_1(\bar{a}_{CoO_2}\bar{a}_{Li^+})^{\alpha_{LiCoO_2}}(\bar{a}_{LiCoO_2})^{(1-\alpha_{LiCoO_2})} \end{aligned} \quad [8]$$

in which $k^s_1 = (k^0_1)^{(1-\alpha_{LiCoO_2})}(k^0_{-1})^{\alpha_{LiCoO_2}}$ is the standard rate constant for reaction Eq. 1.

If an overpotential $\eta^{ct}_{LiCoO_2} = E_{LiCoO_2} - E^{eq}_{LiCoO_2}$ is applied to drive the charge transfer (^{ct}) reaction at the positive electrode, then Eqs. 5a and 5b can be rewritten as

$$I_a = FAa^s_{LiCoO_2}k^0_1 e^{\alpha_{LiCoO_2}(F/(RT))E^{eq}_{LiCoO_2}}e^{\alpha_{LiCoO_2}(F/(RT))\eta^{ct}_{LiCoO_2}} \quad [9a]$$

$$I_c = FAa^s_{CoO_2}a^s_{Li^+}k^0_{-1}e^{-(1-\alpha_{LiCoO_2})(F/(RT))E^{eq}_{LiCoO_2}}e^{-(1-\alpha_{LiCoO_2})(F/(RT))\eta^{ct}_{LiCoO_2}} \quad [9b]$$

Combining the partial cathodic and partial anodic current–potential curves, $I = I_a - I_c$ yields an expression for the kinetics of the charge transfer reaction at the positive electrode. When, in addition, the exchange current, as represented by Eq. 8, is introduced, the following current–potential dependence is obtained

$$I_{LiCoO_2} = I^0_{LiCoO_2}\left[\frac{a^s_{LiCoO_2}}{\bar{a}_{LiCoO_2}}e^{\alpha_{LiCoO_2}(F/(RT))\eta^{ct}_{LiCoO_2}} - \frac{a^s_{CoO_2}a^s_{Li^+}}{\bar{a}_{CoO_2}\bar{a}_{Li^+}}e^{-(1-\alpha_{LiCoO_2})(F/(RT))\eta^{ct}_{LiCoO_2}}\right] \quad [10]$$

Under fully kinetically controlled conditions, $a^s_{CoO_2}a^s_{Li^+}/\bar{a}_{CoO_2}\bar{a}_{Li^+} \approx 1$ and $a^s_{LiCoO_2}/\bar{a}_{LiCoO_2} \approx 1$ and Eq. 10 can be simplified to the Butler–Volmer equation

$$I_{LiCoO_2} = I^0_{LiCoO_2}\left[e^{\alpha_{LiCoO_2}(F/(RT))\eta^{ct}_{LiCoO_2}} - e^{-(1-\alpha_{LiCoO_2})(F/(RT))\eta^{ct}_{LiCoO_2}}\right] \quad [11]$$

In a similar way, the kinetics of the second electrode reaction Eq. 2 can be derived. The general expression for the charge transfer reaction at the metallic lithium electrode can be represented by

$$I_{Li} = I^0_{Li}\left[\frac{a^s_{Li}}{\bar{a}_{Li}}e^{\alpha_{Li}(F/(RT))\eta^{ct}_{Li}} - \frac{a^s_{Li^+}}{\bar{a}_{Li^+}}e^{-(1-\alpha_{Li})(F/(RT))\eta^{ct}_{Li}}\right] \quad [12]$$

where a^s_{Li} and $\bar{a}_{Li}$ are the surface and bulk activities of the metallic Li (mol m^{-3}), α_{Li} is the charge transfer coefficient for reaction Eq. 2, η^{ct}_{Li} is the overpotential of the charge transfer reaction at the negative electrode, and the exchange current I^0_{Li} is given by

$$I^0_{Li} = FAk^s_2(\bar{a}_{Li^+})^{\alpha_{Li}}(\bar{a}_{Li})^{(1-\alpha_{Li})} \quad [13]$$

where k^s_2 is the standard rate constant for reaction Eq. 2. Obviously, the activity of metallic lithium is considered unity. Furthermore, it has been reported that the exchange current density for the metallic lithium electrodes[17] is much larger than that for $LiCoO_2$ [18,19] and because the electrode areas are exactly the same for planar thin-film batteries it is to be expected that η^{ct}_{Li} is much smaller than $\eta^{ct}_{LiCoO_2}$. For convenience, the charge transfer kinetics of the metallic lithium reaction will therefore be neglected in this work.

Diffusion and migration in the electrolyte.— The Li_3PO_4-based solid-state electrolyte is a typical ionic conductor in which the conductivity is caused by the transport of Li^+ ions only. Lithium oxide–phosphorus pentoxide (Li_2O–P_2O_5) is a classical glass-forming system. It is known that a quasi-two-dimensional polymeric network of P_2O_5 is depolymerized in the presence of a modifier, such as Li_2O.[20,21] This Li_2O-induced modification results in converting the bridging oxygen atoms to nonbridging oxygen atoms (nBO's).[22] The "weak electrolyte" models conclude that Li may reside in the two types of states in the glass matrix and assume that the ionic conduction process is dominated by the ions, thermally populating the higher energy (mobile) sites.[23-25] The chemical reaction of the ionization reaction

$$Li^0 \underset{k_r}{\overset{k_d}{\rightleftarrows}} Li^+ + n^- \quad [14]$$

describes the transfer process of immobile, oxygen-binded lithium (indicated by Li^0) to mobile Li^+ ions leaving uncompensated negative charges (n^-) behind, which are chemically associated with the closest nBO's.[22] In Eq. 14, k_d is the dissociation rate constant for the ionic generation reaction (s^{-1}) and k_r is the rate constant for the inverse recombination reaction ($m^3\ mol^{-1}\ s^{-1}$). Both constants obey Arrhenius law. Denoting the activity of mobile Li^+ ions by a_{Li^+} (mol m^{-3}), the activity of immobile Li ions by a_{Li^0} (mol m^{-3}), the activity of n^- by a_{n^-} (mol m^{-3}), the total activity of Li atoms in the Li_3PO_4 matrix by a_0 (mol m^{-3}), and the fraction of Li, which resides in equilibrium in the mobile state by δ, the equilibrium activity of the charge carriers can be represented by $a^{eq}_{Li^+} = a^{eq}_{n^-} = \delta a_0$. The equilibrium activity of immobile lithium is consequently given by $a^{eq}_{Li^0} = (1 - \delta)a_0$. Under equilibrium conditions, the rates of the forward and backward reactions are equal ($k_d a^{eq}_{Li^0} = k_r a^{eq}_{Li^+} a^{eq}_{n^-}$), which implies that $k_d = k_r a_0 \delta^2/(1 - \delta)$. The overall rate of the charge carrier generation is given by $r_d = k_d a_{Li^0} - k_r a_{Li^+} a_{n^-}$, and the net rate of the inverse reaction is given by the opposite number.

The net current passing the electrode/electrolyte interface induces an ionic mass and charge transport in the electrolyte. In the case of a flat geometry, it is reasonable to assume that the ionic transport in the electrolyte is also a one-dimensional process, which can be described by the Nernst–Planck equation[26]

$$J_j = -D_j \frac{\partial a_j}{\partial y} + \frac{z_j F}{RT} D_j a_j E \quad [15]$$

where $J_j(y,t)$ is the flux of species j (mol $m^{-2}\ s^{-1}$) at a distance y from the surface of the negative electrode at any moment in time t, D_j is the diffusion coefficient of j ($m^2\ s^{-1}$), $\partial a_j/\partial y$ is the concentration gradient (mol m^{-4}), E is the potential gradient (V m^{-1}), z_j is the valence (dimensionless), and a_j is the activity (mol m^{-3}) of species j. The two terms on the right-hand side of Eq. 15 represent the diffusion and migration contributions to the ionic flux.

Denoting $r_d = r$ and $r_r = -r$ where $r = k_d a_{Li^0} - k_r a_{Li^+} a_{n^-}$, it can be shown that the two partial differential equations, describing the diffusion–migration process combined with the generation/recombination reaction Eq. 14, can be represented by

$$\frac{\partial a_{Li^+}}{\partial t} = -\frac{\partial J_{Li^+}}{\partial y} + r \quad [16a]$$

$$a_{Li^+}(y,0) = \delta a_0 \quad [16b]$$

$$J_{Li^+}(0,t) = -\frac{I_{Li}(t)}{z_{Li^+} FA} \quad [16c]$$

$$J_{Li^+}(L,t) = \frac{I_{LiCoO_2}(t)}{z_{Li^+} FA} \quad [16d]$$

and

$$\frac{\partial a_{n^-}}{\partial t} = -\frac{\partial J_{n^-}}{\partial y} + r \quad [17a]$$

$$a_{n^-}(y,0) = \delta a_0 \quad [17b]$$

$$J_{n^-}(0,t) = 0 \quad [17c]$$

$$J_{n^-}(L,t) = 0 \quad [17d]$$

where $I_{LiCoO_2}(t)$ and $I_{Li}(t)$ are the charge transfer currents at the positive and negative electrodes, respectively. Equations 16a and 17a represent the mass balances, Eqs. 16b and 17b reflect the fact that at $t = 0$ no concentration profiles have been developed yet and hence that the activities of the charge carriers are equal to their equilibrium activities. Equations 16c, 16d, 17c, and 17d represent the flux conditions at the left and right boundaries of the electrolyte (see also Fig. 1b). Assuming that no side reactions take place, the current flowing through the battery can simply be represented by $I(t) = I_{LiCoO_2}(t) = -I_{Li}(t)$. Equations 16 and 17 accommodate diffusion and migration of both charge carriers. In line with Eq. 15, the flux of each charge carrier is considered independently. Equations 16 and 17 are solved under the electroneutrality condition $a(y,t) = a_{n^-}(y,t) = a_{Li^+}(y,t)$. The Li^+ ions in the electrolyte are generated from the immobile Li atoms, thus $a_0 = a_{Li^0}(y,t) + a_{Li^+}(y,t) = a_{Li^0}(y,t) + a(y,t)$. It can be shown[27] that Eqs. 16 and 17 can be reduced to the diffusion equation with respect to $a(y,t)$, according to

$$\frac{\partial a}{\partial t} = \frac{2D_{Li^+}D_{n^-}}{D_{Li^+} + D_{n^-}} \frac{\partial^2 a}{\partial y^2} + r$$

$$a(y,0) = \delta a_0$$

$$\frac{\partial a(0,t)}{\partial y} = \frac{I(t)}{2FAD_{Li^+}}$$

$$\frac{\partial a(L,t)}{\partial y} = \frac{I(t)}{2FAD_{Li^+}} \quad [18]$$

and an analytical expression for the electric field is obtained

$$E(y,t) = \frac{RT}{F}\frac{1}{a(y,t)}\left\{-\frac{I(t)}{2FAD_{Li^+}} + \frac{D_{Li^+} - D_{n^-}}{D_{Li^+} + D_{n^-}}\left[\frac{\partial a(y,t)}{\partial y} - \frac{I(t)}{2FAD_{Li^+}}\right]\right\} \quad [19]$$

The total mass-transfer (^{mt}) overpotential across the Li_3PO_4 electrolyte $\eta^{mt}_{Li^+}$ can then be given by

$$\eta^{mt}_{Li^+}(t) = \frac{RT}{F}\ln\left[\frac{a(L,t)}{a(0,t)}\right] - \int_0^L E(y,t)dy \quad [20]$$

The first and the second terms in Eq. 20 define the diffusion and migration components of the total overpotential, respectively.

Diffusion in the electrode.— The positive electrode consists of trivalent cobaltoxide species, in which the lithium ions are intercalated ($LiCo^{III}O_2$). According to Refs. 28 and 29 Li^+ ions in $LiCoO_2$ are screened by the mobile electrons, which accompany Li^+ when it moves from one interstitial site to the other. This screening implies that the migration term can be neglected. Assuming, for simplicity reasons, that the rate of phase transition does not play an important role and considering the diffusion coefficients in both phases to be equal, the mass transport of Li ions inside the positive electrode can be described by the standard diffusion equation

$$\frac{\partial a_{LiCoO_2}}{\partial t} = D_{Li}\frac{\partial^2 a_{LiCoO_2}}{\partial y^2} \quad [21a]$$

$$a_{LiCoO_2}(y,0) = a^0_{LiCoO_2} \quad [21b]$$

$$D_{Li}\frac{\partial a_{LiCoO_2}(L,t)}{\partial y} = \frac{I(t)}{FA} \quad [21c]$$

$$D_{Li}\frac{\partial a_{LiCoO_2}(L+M,t)}{\partial y} = 0 \quad [21d]$$

where $a_{LiCoO_2}(y,t)$ is the Li^+ activity (mol m^{-3}) in location y at any moment of time t, $a^0_{LiCoO_2}$ is the activity of Li^+ (mol m^{-3}) in the positive electrode at $t = 0$ (in equilibrium), and D_{Li} is the diffusion

Table I. List of symbols.

Notation	Dimension	Description
L	m	Thickness of the electrolyte
M	m	Thickness of the electrode
A	m^2	Geometrical surface area
a^s	mol m^{-3}	Generic notation for surface activity
$\bar{a}$	mol m^{-3}	Generic notation for bulk activity
a_{LiCoO_2}	mol m^{-3}	Activity of Li in the positive ($LiCoO_2$) electrode (generic)
a_{Li}	mol m^{-3}	Activity of Li in the negative (metallic Li) electrode (generic)
a_{Li^+}	mol m^{-3}	Activity of Li^+ in the electrolyte (generic)
a_{n^-}	mol m^{-3}	Activity of n^- in the electrolyte (generic)
a_{Li^0}	mol m^{-3}	Activity of immobile lithium in Li_3PO_4 matrix
a_0	mol m^{-3}	Total activity of Li atoms in Li_3PO_4 matrix
k_1	m s^{-1}	Positive electrode charge transfer anodic reaction rate constant
k_{-1}	m^4 mol^{-4} s^{-1}	Positive electrode charge transfer cathodic reaction rate constant
k_1^s	$m^{2.8}$ $mol^{-0.6}$ s^{-1}	Standard rate constant for positive electrode charge transfer reaction
k_2	m s^{-1}	Negative electrode charge transfer anodic reaction rate constant
k_{-2}	m s^{-1}	Negative electrode charge transfer cathodic reaction rate constant
k_2^s	m s^{-1}	Standard rate constant for negative electrode charge transfer reaction
k_r	m^3 mol^{-1} s^{-1}	Li^+ ion recombination reaction rate constant
k_d	s^{-1}	Li^+ ion generation reaction rate constant
r	mol s^{-1}	Net rate of Li^+ ion generation/recombination
δ	—	Fraction of mobile Li^+ ions in the electrolyte in equilibrium
D_{Li^+}	m^2 s^{-1}	Diffusion coefficient for Li^+ ions in the electrolyte
D_{n^-}	m^2 s^{-1}	Diffusion coefficient for n^- in the electrolyte
D_{Li}	m^2 s^{-1}	Diffusion coefficient for Li in the positive electrode
J_j	mol m^{-2} s^{-1}	Flux of species j in the electrolyte
z_j	—	Valence of species j
I_{LiCoO_2}, I_{Li}	A	Main storage reaction currents for the positive and negative electrode correspondingly
I	A	Current flowing through the battery
$I^0_{LiCoO_2}$, I^0_{Li}	A	Exchange currents for the positive and negative electrodes correspondingly
I_a, I_c	A	Anodic and cathodic currents for the charge transfer reactions
E_{LiCoO_2}, $E^{eq}_{LiCoO_2}$	V	Voltage and equilibrium voltage of the positive electrode
E_{bat}, E^{eq}_{bat}	V	Voltage and equilibrium voltage of the battery
E	V m^{-1}	Electric field (electric potential gradient)
η	V	Total overpotential of the battery
$\eta^{ct}_{LiCoO_2}$	V	The charge transfer overpotential for the positive electrode
$\eta^{mt}_{Li^+}$	V	The mass-transfer overpotential across the electrolyte
$\eta^{d}_{LiCoO_2}$	V	The diffusion overpotential for the positive electrode
T	K	Temperature
t	s	Time

coefficient (m^2 s^{-1}) of Li in the electrode. Equation 21a represents how the profile develops as a function of time. Equation 21b reflects the initial conditions and Eq. 21c describes the supply or consumption of the Li^+ ions at the electrode interface. Equation 21d reveals the insulating condition at the electrode/current collector interface ($y = L + M$ in Fig. 1b) through which no Li^+ ions can pass. Note that the normalized activity of Li in the electrode can be defined as $x = a_{LiCoO_2}/a^{max}_{LiCoO_2}$, where $a^{max}_{LiCoO_2}$ is the maximal activity of Li in $LiCoO_2$ (23.3 kmol m^{-3}). The diffusion overpotential is calculated according to Refs. 28 and 30 as $\eta^d_{LiCoO_2} = E^{eq}_{LiCoO_2}(x^s) - E^{eq}_{LiCoO_2}(\bar{x}) \approx (x^s - \bar{x})(\partial E^{eq}_{LiCoO_2}/\partial x)$, where $x^s = x(L,t)$ is the normalized surface activity, $\bar{x}$ is the average bulk activity, and $\partial E^{eq}_{LiCoO_2}/\partial x$ is the derivative of the equilibrium potential of the positive electrode at the surface.

Combined effects.— The equilibrium voltage of the Li-ion battery is the difference between the equilibrium voltage of the positive and negative electrodes, i.e., $E^{eq}_{bat} = E^{eq}_{LiCoO_2} - E^{eq}_{Li}$. The total battery overpotential (η) is the difference between the equilibrium voltages and the current-driven voltages ($\eta = E_{bat} - E^{eq}_{bat}$). The total battery overpotential (η_t) is a sum of three contributions

$$\eta_t = \eta^{ct}_{LiCoO_2} + \eta^{d}_{LiCoO_2} + \eta^{mt}_{Li^+} \quad [22]$$

according to the three main processes occurring inside the battery: the charge transfer reaction at the positive electrode, the ionic flow through the solid-state electrolyte, and the diffusion in the intercalation electrode. Herewith, it is indeed assumed that η^{ct}_{Li} at the metallic lithium electrode is negligibly low. Table I lists all model parameters.

Experimental

A 10 μAh planar thin-film all-solid-state Li-ion battery was deposited using an in-house built equipment, comprising a radio frequency sputtering tool with 2 in. targets (13.56 MHz) and thermal/E-beam evaporation, both placed in a glove box containing an inert argon atmosphere. Care was taken that the base pressure before deposition was always less than 10^{-6} mbar. Hard masks were used for the definition of each of the active battery layers. As substrate, silicon covered with a bistack of TiO_2/Pt (50 nm/250 nm) was used. For the cathode ($LiCoO_2$ target), a power of 60 W and a pressure of 8×10^{-6} bar O_2/Ar (4:6) were used to deposit 320 nm. Hereafter, the cathode was thermally annealed at 800°C for 10 min using rapid thermal anneal at a 60°C/min heating rate in order to obtain the high-T crystalline phase. Hereafter, a 1.5 μm thick

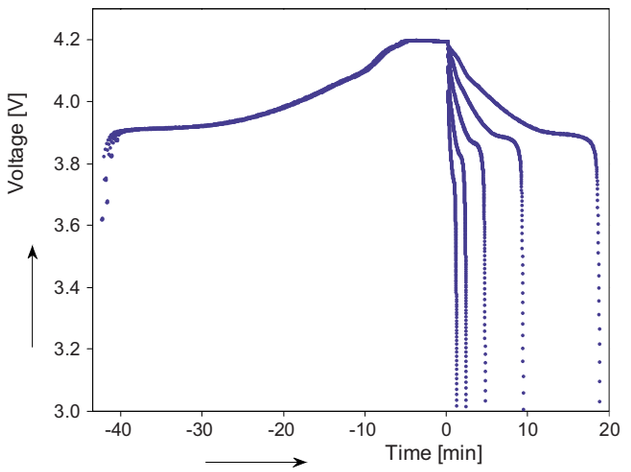

Figure 2. (Color online) Experimentally measured voltage profiles during CCCV charging (CC = C-rate; V_{max} = 4.2 V), relaxation and discharging at various C-rates (3.2, 6.4, 12.8, 25.6, and 51.2 C-rate).

Li_3PO_4 layer was deposited using a power of 30 W using a Li_3PO_4 target (at a pressure of 15×10^{-6} bar Ar). Finally, 150 nm cobalt was deposited as the current collector at ~5 Å/s via E-beam evaporation. The as-prepared battery was charged and discharged according to the following regime: constant current constant voltage (CCCV) charging with a 1.6 C-rate till the maximum voltage level of 4.2 V was reached, followed by a 30 min relaxation period and a current constant (CC) discharge. The following discharge rates were successively applied: 1.6, 3.2, 6.4, 12.8, 25.6, and 51.2 C. Cycling was performed on an 8-channel Biologic VMP3 battery tester equipped with a low current and impedance boards. The experimental data are obtained at room temperature, i.e., 25°C, the same temperature as used for the simulations.

Results and Discussion

Figure 2 shows the charge and discharge voltage curves as a function of time where, for convenience reasons, $t = 0$ corresponds to the start of each discharge cycle. It is remarkable to see that these thin-film batteries can be discharged with extremely high currents up to 51.2 C-rate.

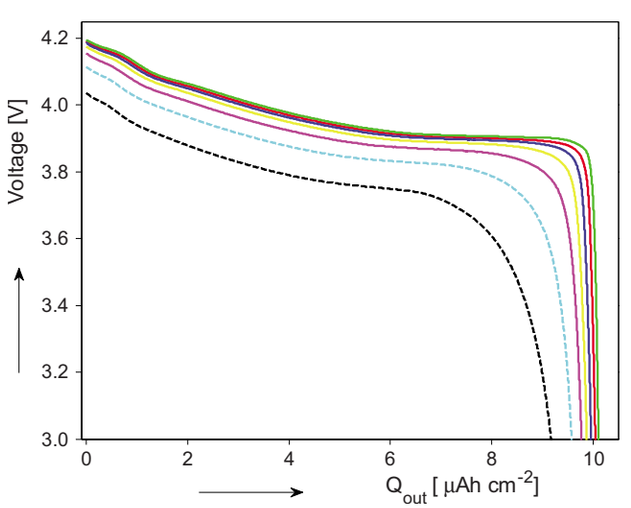

Figure 3. (Color online) Equilibrium voltage (green) obtained from extrapolation and experimentally measured discharge curves (1.6, 3.2, 6.4, 12.8, 25.6, and 51.2 C-rate).

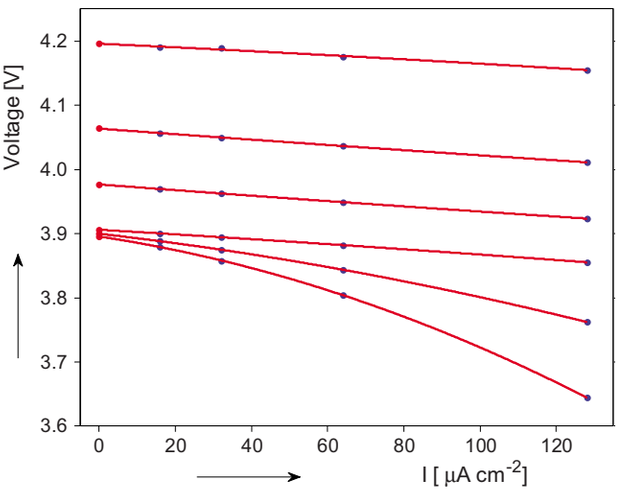

Figure 4. (Color online) The blue symbols are measured voltages at various values of Q_{out}; The red line is the regression interpolation; The red dots represent the extrapolated equilibrium voltage. The curves were obtained at Q_{out} = 0, 2, 4, 8, 9.25, and 9.50 µAh cm^{-2}.

Figure 3 shows the same discharge curves but now plotted as a function of the amount of extracted charge (Q_{out}), i.e., capacity density, together with the extrapolated equilibrium voltage curve (green line). Note that the equilibrium voltage of the battery is equal to that of the positive electrode as the voltage of the metallic Li electrode is 0 V vs Li/Li$^+$, i.e., $E^{eq}_{bat} = E^{eq}_{LiCoO_2}$. The equilibrium voltage has been determined by regression extrapolation (see Chap. 4 in Ref. 31). The regression extrapolation was applied separately on the flat and steep parts of the equilibrium voltage curve. Figure 4 shows, as an example, the dependence of the voltage on the applied discharge current for six different values of Q_{out}. A linear relationship between the current density and voltage is found for the low Q_{out} values up to 8 µAh cm^{-2}. At low state-of-charges, a nonlinear dependence is found, which can be well approximated by a quadratic regression model. The steep part of the equilibrium voltage curve has been obtained by applying a regression model to the set of Q_{out} and current densities. By extrapolating the currents to zero, the equilibrium voltage can be determined. Figure 5 shows the dependence of Q_{out}

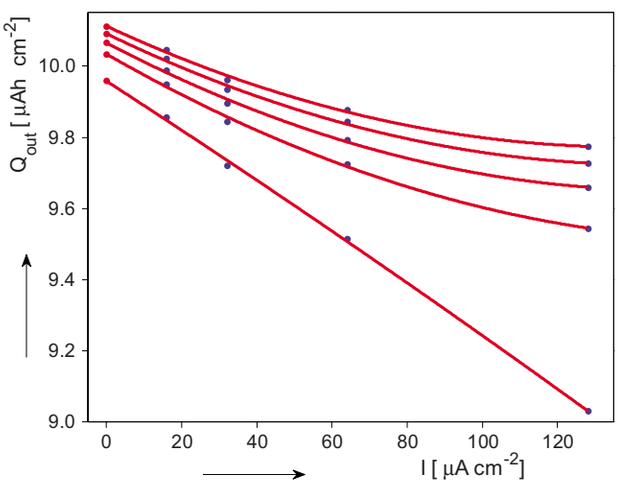

Figure 5. (Color online) The blue symbols are measured Q_{out} values as a function of discharge current; The red line is the regression interpolation; The red symbols represent the extrapolated Q_{out} values. The curves are obtained at V = 3.0, 3.2, 3.4, 3.6, and 3.8 V.

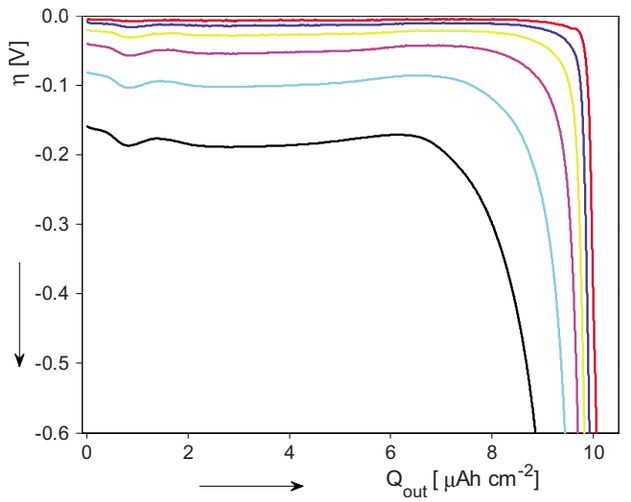

Figure 6. (Color online) Experimental overpotentials as a function of Q_{out} at various C-rates (from 1.6 to 51.2 C-rate).

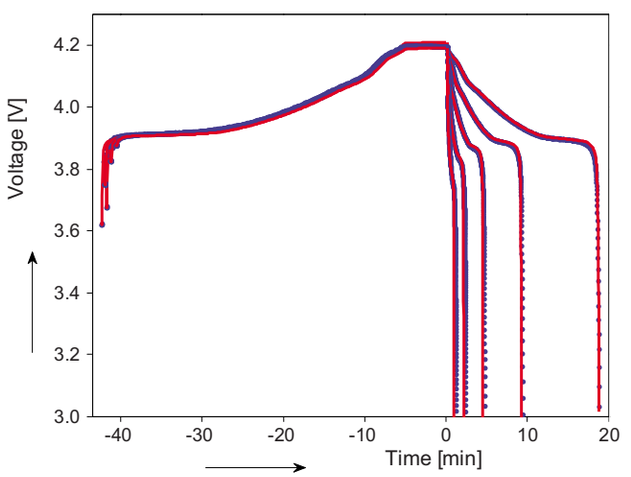

Figure 7. (Color online) Overall performance of the model during discharges with various C-rates. The blue symbols are measurements and, the red lines are the model predictions.

on the applied discharge current at five different voltages. For all voltages, nonlinear dependencies between Q_{out} and the applied current are found, which have been approximated by a quadratic regression. Q_{out} can then be found by extrapolating toward zero current.

The difference between the equilibrium voltage and the discharge voltage is the overpotential. The dependence of the total experimental overpotential as a function of Q_{out} at various discharge rates is shown in Fig. 6. For all currents, a wide flat plateau is followed by a sharp decrease at the end of the discharge process.

Figure 7 shows the optimized simulations obtained with the applied model. Good agreement is obtained between the experimental results (blue dots) and the theoretical prediction (red lines) for all (dis)charge currents. The optimized parameters are listed in Table II.

Figure 8a shows the contributions of the various overpotential components during discharging at 3.2 C-rate. It is evident that the diffusion overpotential at the $LiCoO_2$ electrode ($\eta^{d}_{LiCoO_2}$) provides the largest contribution at the beginning of discharging, but reduces toward zero, except at the very end of the discharge process where it increases sharply due to the steep concentration gradient of Li ions in the cathode. The mass-transfer overpotential ($\eta^{mt}_{Li^+}$) of the electrolyte is the second in magnitude at the beginning of discharging, but dominates in the end. The charge transfer overpotential ($\eta^{ct}_{LiCoO_2}$) is initially small but is growing significantly toward the end of the discharge process.

Similarly, a high discharge rate of 51.2 C (Fig. 8b) induces a high mass-transfer overpotential ($\eta^{mt}_{Li^+}$), which is slowly increasing upon discharging. This overpotential across the electrolyte is responsible for at least half of the total overpotential starting from the second half of the discharge process. The diffusion overpotential at the cathode ($\eta^{d}_{LiCoO_2}$) contributes significantly in the beginning and at the very end of the discharge process. This behavior is in-line with the definition of the diffusion overpotential which is proportional to the derivative of the equilibrium voltage (see Diffusion in the electrode). Consequently, the overpotential is small in the second half of the discharge process, where the corresponding equilibrium voltage curve is rather flat and explodes sharply at the very end of the discharge process, where the equilibrium voltage drops rapidly. The simulated total overpotential agrees well with the experimentally determined overpotentials plotted in Fig. 5: in the case of a 51.2 C-rate discharge simulation, a wide overpotential plateau at about −0.2 V is calculated which is in good agreement with the experimentally determined overpotential in Fig. 6 (black line). By carefully checking the various overpotential contributions at the end

Table II. Model parameters.

Parameter	Dimension	Estimated value	Description
L	nm	1500	Thickness of the electrolyte[a]
M	nm	320	Thickness of the electrode[a]
A	cm^2	1	Geometrical surface area[a]
a_0	mol m^{-3}	6.01×10^4	Total activity of Li atoms in Li_3PO_4 matrix[b]
k_r	m^3 mol^{-1} s^{-1}	0.90×10^{-8}	Li^+-ion recombination reaction rate
δ	—	0.18	Fraction of free Li^+ ions in equilibrium
D_{Li^+}	m^2 s^{-1}	0.90×10^{-15}	Diffusion coefficient for Li^+ ions in the electrolyte
D_{n^-}	m^2 s^{-1}	5.10×10^{-15}	Diffusion coefficient for n^- in the electrolyte
$a^{max}_{LiCoO_2}$	mol m^{-3}	2.33×10^4	Maximal activity of Li in the positive electrode[c]
D_{Li}	m^2 s^{-1}	1.76×10^{-15}	Diffusion coefficient for Li in the positive electrode
α_{LiCoO_2}	—	0.6	Charge transfer coefficient for the positive electrode
k^s_1	$m^{2.8}$ $mol^{-0.6}$ s^{-1}	5.1×10^{-6}	Standard rate constant for positive electrode charge transfer reaction

[a] Design parameters.
[b] Outcome of NDP analysis.
[c] Estimated from the design parameters and maximal capacity of the battery. All the remaining parameters are obtained from model optimization.

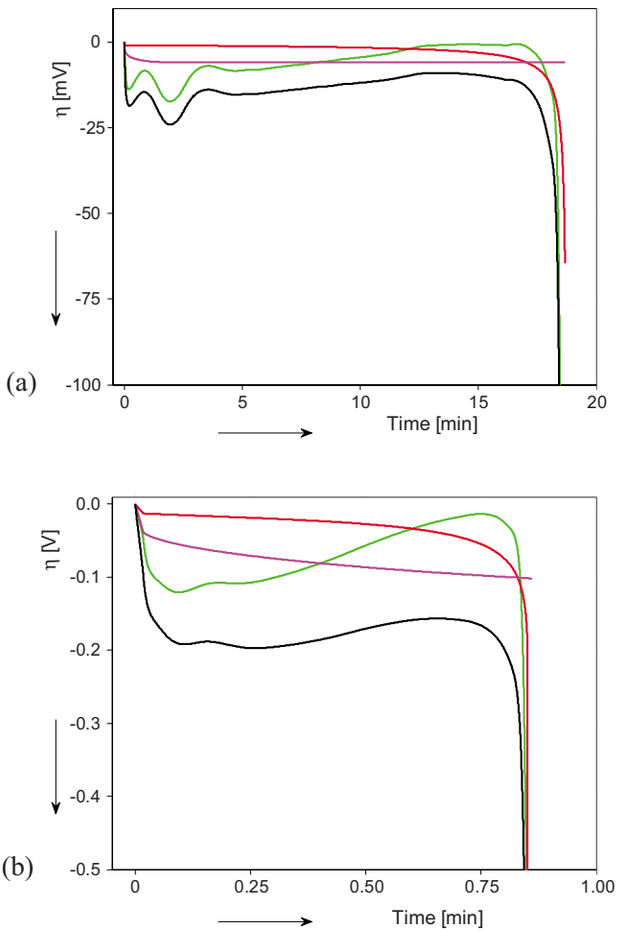

Figure 8. (Color online) Development of the overpotentials as a function of time during low-current (a) and high-current (51.2 C) discharging (b). The red lines represent simulated Butler–Volmer overvoltage ($\eta^{ct}_{LiCoO_2}$), the pink lines represent mass-transfer overpotential in the electrolyte ($\eta^{mt}_{Li^+}$), and the green lines represent diffusion overpotential in the solid-state electrode ($\eta^{d}_{LiCoO_2}$). The black lines are the total simulated overvoltage, i.e., the summation of the three individual components (η_t).

of the discharge process, it becomes clear that diffusion inside the $LiCoO_2$ electrode is the leading process, inducing the current interruption at the battery cutoff voltage of 3.0 V.

Figure 9 shows in more detail the development of the Li-ion concentration profile in the $LiCoO_2$ electrode upon discharging at a high 51.2 C-rate. Starting at $t = 0$, the system is at equilibrium and no concentration gradient has been built up yet. As soon as a discharge current is applied, a concentration profile is built up across the $LiCoO_2$ electrode, increasing more rapidly at the electrode/electrolyte interface. This is in good agreement with the Li-intercalation reaction Eq. 1, which indeed reveals an influx of Li ions into the positive electrode during discharging. The diffusion coefficient for Li in the electrode has been analyzed to be 1.76×10^{-15} m^2 s^{-1}, which also agrees well with the reported experimental results.[32,33] After about 1 min, the current is switched off and the concentration profile quickly relaxes toward the equilibrium.

The evolution of the concentration profile of Li^+ ions across the electrolyte upon high current discharging is shown in Fig. 10. Starting from a flat concentration profile at equilibrium, a steep increase of the Li^+-concentration is found at the metallic Li/electrolyte interface (at $y = 0$, see also Fig. 1b), while at the $LiCoO_2$/electrolyte interface ($y = L$) the concentration becomes rather low. When the

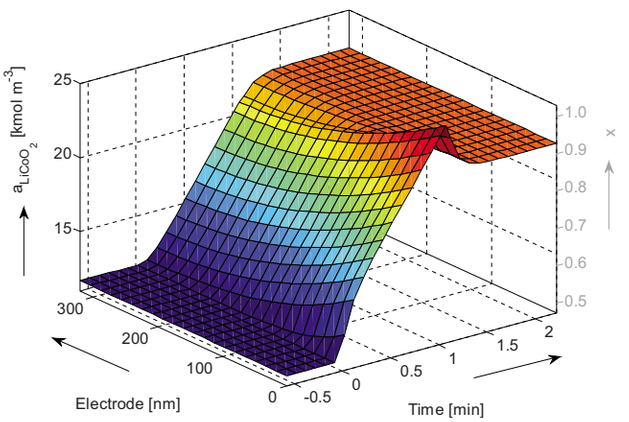

Figure 9. (Color online) Development of the Li-concentration profile inside the positive electrode during 51.2 C discharge.

discharge current is switched off after 1 min, the concentration profiles rapidly relax to their equilibrium value of 11 kmol m^{-3}.

Figure 11 shows the development of the total overpotential (pink line) and the individual contributions of diffusion (red line) and migration (blue line) at 51.2 C-rate discharging. The equilibrium situation ($t < 0$) corresponds to a zero overpotential. When the current is switched on, a 40 mV voltage drop is instantaneously formed, which is fully carried by the electric field as no concentration gradient has been built up yet. This rapid initial increase is followed by a more steady increase of both migration and diffusion, in total amounting to 110 mV at the end of discharging. The thicknesses of the electrode (M) and the electrolyte (L) have been determined by scanning electron microscopy (SEM). The total number of Li in the Li_3PO_4 electrolyte has been analyzed by neutron depth profiling (NDP) to be $a_0 = 6.01 \times 10^4$ mol m^{-3}. The simulations show that, in equilibrium, only about 18% of the Li atoms are mobile and that the Li-ion recombination reaction rate is moderately large ($k_r = 0.9 \times 10^{-8}$ m^3 mol^{-1} s^{-1}). Both diffusion coefficients are estimated to be of the order of 10^{-15} m^2 s^{-1}.

Figure 12 reviews the concentration profiles across the entire battery stack at three moments in time: directly preceding constant current-discharging (blue line), 20 s after 51.2 C-rate discharging has been commenced (red line), and after 50 s (pink line) just before discharging will be terminated. It can be concluded that before discharging no concentration profiles are present in both the electrode

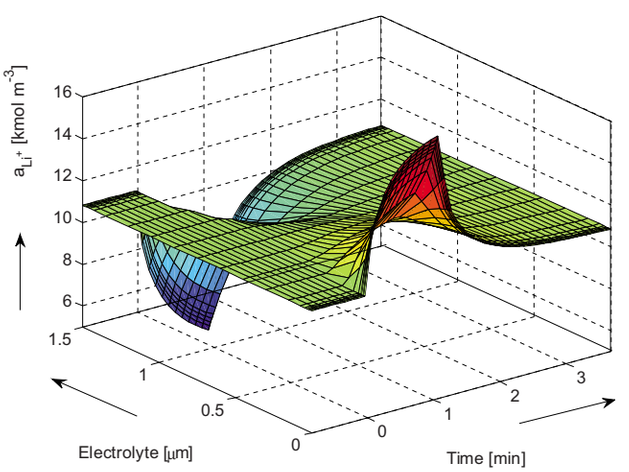

Figure 10. (Color online) Development of the Li-concentration profile inside the electrolyte layer during 51.2 C discharge.

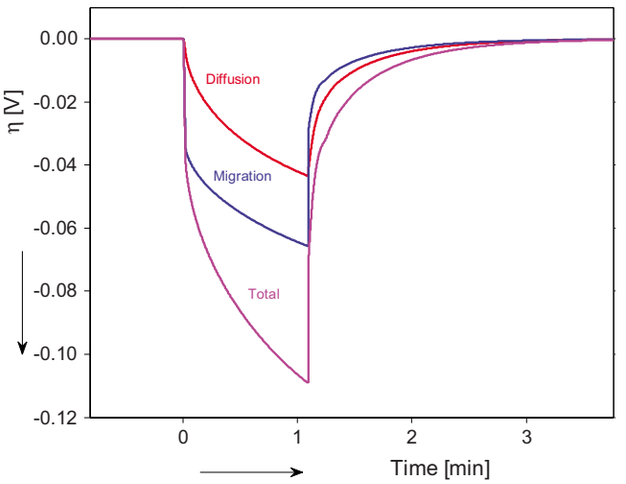

Figure 11. (Color online) Development of the overpotentials across the electrolyte layer during 51.2 C discharge: diffusion (red line), migration (blue line), and summation of those two, total (pink line).

and the electrolyte, indeed implying that the battery is in the equilibrium state. However, as soon as the current is switched on, significant concentration gradients in both the electrode and the electrolyte are established, with significant accumulation at the metallic lithium electrode ($y = 0$) and depletion at the electrolyte/cathode interface ($y = L$). The lithium concentration in the positive electrode, conversely, is growing with time, in agreement with the main storage reaction Eq. 1. The simulated total overpotential corresponds to charge transfer resistances of the order of 50–100 Ω at the voltage plateau but obviously increases at the end of discharging. This is also in good agreement with the reported experimental results.[18,19]

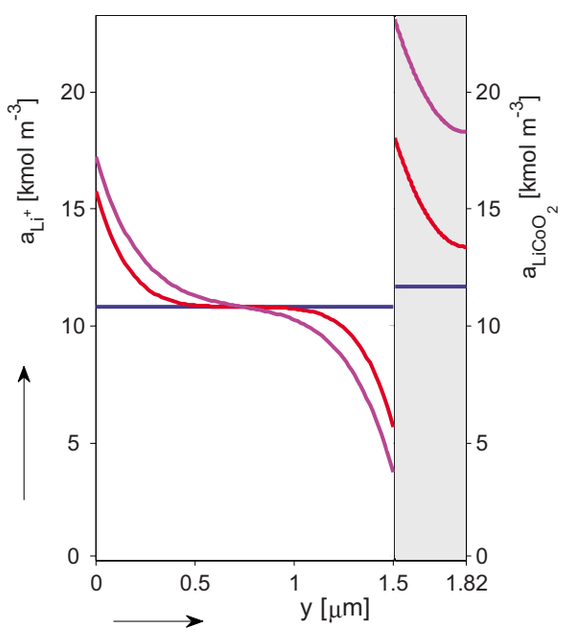

Figure 12. (Color online) Concentration profiles in the complete battery stack before discharging (51.2 C-rate) has been commenced (blue), in the middle of the discharge process (red), and just before the discharge current will be terminated (pink). The electrolyte is at the left, the $LiCoO_2$ electrode is indicated by the shaded area.

Conclusions

A one-dimensional model has been applied to simulate the performance of all-solid-state Li-ion batteries. The model describes the electrode, electrolyte, and the interface between those elements. The proposed model provides a detailed information about the various diffusion and migration fluxes, concentration profiles, and the corresponding overpotential contributions, occurring across the electrode and electrolyte. The model provides good fits with the measurements, including discharge curves with high C-rates.

Acknowledgments

The authors thank Dr. H.T. Hintzen (Eindhoven University of Technology) and Dr. I. Kokal for their valuable discussions. The work has been supported by the European Union (FP7) within the framework of the Superlion project.

Eindhoven University of Technology assisted in meeting the publication costs of this article.

References

1. M. Doyle, T. F. Fuller, and J. Newman, *J. Electrochem. Soc.*, **140**, 1526 (1993).
2. C. R. Pals and J. Newman, *J. Electrochem. Soc.*, **142**, 3274 (1995).
3. L. Song and J. W. Evans, *J. Electrochem. Soc.*, **147**, 2086 (2000).
4. G. G. Botte, V. R. Subramanian, and R. E. White, *Electrochim. Acta*, **45**, 2595 (2000).
5. P. M. Gomadam, J. W. Weidner, R. A. Dougal, and R. E. White, *J. Power Sources*, **110**, 267 (2002).
6. J. S. Newman, *Electrochemical Systems*, Prentice-Hall, Englewood Cliffs, NJ (1991).
7. W. S. Kruijt, P. H. L. Notten, and H. J. Bergveld, *J. Electrochem. Soc.*, **145**, 3764 (1998).
8. P. H. L. Notten, W. S. Kruijt, and H. J. Bergveld, *J. Electrochem. Soc.*, **145**, 3774 (1998).
9. H. J. Bergveld, W. S. Kruijt, and P. H. L. Notten, *J. Power Sources*, **77**, 143 (1999).
10. W. S. Kruijt, E. de Beer, P. H. L. Notten, and H. J. Bergveld, Abstract 104, The Electrochemical Society Meeting Abstracts Vol. 97-1, Paris, France, p. 114 (1997).
11. H. J. Bergveld, W. S. Kruijt, and P. H. L. Notten, *Battery Management Systems—Design by Modelling*, Philips Research Book Series, Vol. 1, Kluwer Academic Publishers, Boston (2002).
12. D. Danilov and P. H. L. Notten, Abstract 390, in Proceedings of the 12th IMLB Conference, Nara, Japan, 2004.
13. D. Danilov and P. H. L. Notten, in *Proceedings of the 5th IEEE Vehicle Power and Propulsion Conference*, IEEE, Dearborn, p. 317 (2009).
14. J. B. Bates, N. J. Dudney, G. R. Gruzalski, R. A. Zuhr, A. Choudhury, C. F. Luck, and J. D. Robertson, *J. Power Sources*, **43**, 103 (1993).
15. J. B. Bates, N. J. Dudney, D. C. Lubben, G. R. Gruzalski, B. S. Kwak, Y. Xiaohua, and R. A. Zuhr, *J. Power Sources*, **54**, 58 (1995).
16. P. H. L. Notten, in *Interstitial Intermetallic Alloys*, F. Grandjean, G. J. Long, and K. H. J. Buschow, Editors, Chap. 7, p. 151 Kluwer, Dordrecht (1995).
17. N. Munichandraiah, L. G. Scanlon, and R. A. Mars, *J. Power Sources*, **72**, 203 (1998).
18. Y. Iriyama, T. Kako, C. Yada, T. Abe, and Z. Ogumi, *J. Power Sources*, **146**, 745 (2005).
19. I. Yamada, Y. Iriyama, T. Abe, and Z. Ogumi, *J. Power Sources*, **172**, 933 (2007).
20. J. R. van Wazer, *Phosphorus and its Compounds*, Vol. 1, Interscience, New York (1958).
21. S. W. Martin, *Eur. J. Solid State Inorg. Chem.*, **28**, 163 (1991).
22. H. Kahnt, *J. Non-Cryst. Solids*, **203**, 225 (1996).
23. M. D. Ingram, C. T. Moynihan, and A. V. Lesikar, *J. Non-Cryst. Solids*, **38-39**, 371 (1980).
24. D. Ravaine and J. L. Souquet, *Phys. Chem. Glasses*, **18**, 27 (1977).
25. S. W. Martin and C. A. Angell, *J. Non-Cryst. Solids*, **83**, 185 (1986).
26. A. J. Bard and L. R. Faulkner, *Electrochemical Methods, Fundamentals and Applications*, John Wiley & Sons, New York (1980).
27. D. Danilov and P. H. L. Notten, *Electrochim. Acta*, **53**, 5569 (2008).
28. W. R. McKinnon and R. R. Haering, in *Modern Aspects of Electrochemistry*, Vol. 15, R. E. White, J. O. M. Bockris, and B. E. Conway, Editors, Chap. 4, p. 235, Plenum, New York (1983).
29. K. Kang and G. Ceder, *Phys. Rev. B*, **74**, 094105 (2006).
30. S. Atlung, K. West, and T. Jacobsen, *J. Electrochem. Soc.*, **126**, 1311 (1979).
31. V. Pop, H. J. Bergveld, D. Danilov, P. P. L. Regtien, and P. H. L. Notten, *Battery Management Systems: Accurate State-of-Charge Indication for Battery-Powered Applications*, Philips Research Book Series, Vol. 9, Springer, New York (2008).
32. J. Xie, N. Imanishi, A. Hirano, M. Matsumura, Y. Takeda, and O. Yamamoto, *Solid State Ionics*, **178**, 1218 (2007).
33. H. Sato, D. Takahashi, T. Nishina, and I. Uchida, *J. Power Sources*, **68**, 540 (1997).